JOURNAL OF MATERIALS SCIENCE **36** (2001) 1641 – 1651

Analysis of failure mechanisms in platelet-reinforced composites

Y. WYSER‡, Y. LETERRIER, J.-A. E. MÅNSON*
Laboratoire de Technologie des Composites et Polymères (LTC), Ecole Polytechnique Fédérale de Lausanne (EPFL), CH-1015 Lausanne, Switzerland
E-mail: yves.leterrier@epfl.ch

The short-term mechanical strength of platelet-reinforced polymer composites was modeled using classical two-dimensional stress-transfer analysis. The stress field in the platelet and at the platelet/matrix interface was described in the presence of a matrix crack perpendicular to the interface. Modeling takes into account the tensile strength of the platelet, its adhesion to the matrix, and also considers the internal stress state resulting from processing. Platelet rupture and interface delamination were considered to be the two key failure mechanisms, depending on the ratio of platelet strength to interface strength. The transition between the two failure events was predicted to occur at a critical platelet length, the value of which depends on the elastic properties of the platelet and matrix, on the platelet geometry and strength, on the platelet/matrix adhesion, and on the internal stress state. The approach was applied to the case of low volume fraction silicon oxide platelets/poly(ethylene terephthalate) composites, where the size of the platelets was accurately controlled either below or above the predicted critical length. Compression molded composites, with perfect alignment of the platelets, and injection molded composites, were prepared and tested. The toughness of the compression molded composites was found to be accurately predicted by the strength model, with a 100% increase in the case of platelets smaller than the critical length compared to larger platelets. Injection molded composites with platelets larger than the critical length were found to fail without yielding. By contrast, when the platelets were smaller than the critical length, the injection molded composites exhibited excellent ductility. The general agreement obtained between the predicted and observed toughening transition shows the importance of filler size and stress state on the strength of platelet-reinforced composites.

1. Introduction

Platelet-reinforced polymer composites are used in a large variety of products, including high-voltage electrical insulators where perfect alignment of mica platelets is required. They also find applications similar to those of fiber-reinforced composites, with the advantage of in-plane isotropy over aligned fibers, however with somewhat reduced strength [1–5]. Ceramic fillers with well defined platelet morphology, such as mica and Al_2O_3, or flake-like shape, like talc and $CaCO_3$, find widespread use as they often provide the advantage of reduced cost while improving stiffness, creep resistance, and reducing the coefficient of thermal expansion. The issue of recycled polymers is also frequently related to contamination problems with non-polymeric impurities, which adversely affect the performance of the reprocessed material. The planar geometry of the platelet/polymer interface is also relevant for microelectronic devices. In these functional applications, multi-material integration generates complex internal stress fields and interface defects which are likely to limit the device performance. The identification of the relevant failure mechanisms at interfaces is more and more recognized as a key factor for ensuring functional durability, particularly when the devices operate at the micrometer scale (see for instance ref. [6]).

Whether in structural or functional applications, the development of polymer composites goes along with the need to predict their mechanical reliability. The mechanics of polymers reinforced with particulate inclusions have been extensively detailed, and it is now established that both the size of the filler and stress state affect the elastic properties of this class of materials, as reviewed for instance in reference [7]. However, the numerous filler/matrix combinations and processing techniques currently available, together

‡ *Present Address*: Nestlé Research Center, Quality and Safety Insurance Departement, Packaging Laboratory, Vers-chez-les-Blanc, 1000 Lausanne 26, Switzerland.
* Author to whom all correspondence should be addressed.

with the often complex geometry of the manufactured product, makes it very difficult to accurately predict the composite strength. The manufacture of any composite material inevitably generates inhomogeneous stress fields and gradients in structure, resulting from polymer flow, pressure, and temperature fields. Their effect on strength and durability is *a priori* unknown. In particular, a central concern in strength analysis is the stress transfer between the matrix and the filler. This issue has been studied by many authors in the case of fiber reinforced composites [8–21], and, to a lesser extent, in the case of particle reinforced composites [22–32]. Most of these works are based on the classical shear-lag theory developed by Cox [33] for fiber geometry. The case of platelet reinforcement has been examined in detail in the field of metal matrix and ceramic matrix composites, particularly when reinforced by Al_2O_3, TiB_2 or SiC platelets, but to a far less extent in the case of polymer matrix composites [5, 34].

Based on the shear stress acting at the interface, and on the axial stress acting on the platelet, a model is proposed in order to analyze the failure mechanisms of platelet-reinforced composites, taking into account the platelet length and the process-induced internal stresses. The approach is applied to silicon oxide platelet-reinforced poly(ethylene terephthalate) composites (PET/SiO_x), compression molded or injection molded, with diluted oxide platelets of different lengths and orientation.

2. Strength analysis of platelet-reinforced composites

The first two-dimensional elastic stress transfer analysis to model the mechanical properties of platelet filled materials was proposed by Tyson and Davis [35], based on the shear lag model developed by Cox [33]. However, the shear stress at the platelet/matrix interface predicted by Tyson and Davis was found to be much lower than that measured experimentally. The following approach is based on a more effective two-dimensional elastic stress transfer model which was derived more recently by Hsueh from the stress equilibrium equation for platelet reinforcement [5, 34].

2.1. Elastic stress transfer analysis at the platelet/matrix interface

The stress transfer between the matrix and the platelet is derived from the equilibrium equation between the axial stress in the platelet and the shear stress at the platelet/matrix interface [36]. The geometry used for this analysis is shown in Fig. 1. A platelet of length $L = 2t$ and thickness 2a is embedded in a matrix element with length 2u and thickness 2b. The tensile stress, σ_0, is applied in the y direction. Assuming that the ends of the platelets are not bonded to the matrix, which implies that all the stress transfer happens through the interface, the axial stress in the platelet, σ, at a distance y from its center, averaged over its thickness, is written as [5]:

$$\sigma = \psi\sigma_0\left[1 - \frac{\exp(\varphi y) + \exp(-\varphi y)}{\exp(\varphi t) + \exp(-\varphi t)}\right] \qquad (1)$$

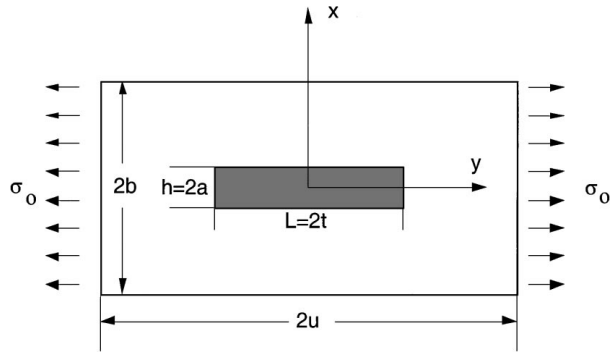

Figure 1 Geometry used for the stress transfer analysis (after reference [5]).

and the interfacial shear stress, τ_p, at the same point:

$$\tau_p = a\varphi\psi\sigma_0\left[\frac{\exp(\varphi y) - \exp(-\varphi y)}{\exp(\varphi t) + \exp(-\varphi t)}\right] \qquad (2)$$

where

$$\varphi = \frac{1}{(b-a)}\sqrt{\left\{\frac{3[aE_p + (b-a)E_m]}{2a(1+\nu_m)E_p}\right\}},$$

E_m being the elastic modulus of the matrix, ν_m being its Poisson's ratio, E_p the modulus of the platelet, and

$$\psi = \frac{bE_p}{aE_p + (b-a)E_m}.$$

The maximum tensile stress, σ_∞, and maximum shear stress, τ_∞, in a platelet of length 2t, appear at the center of the particle and at its edge, respectively. The former is obtained from Equation 1, taking $y = 0$:

$$\sigma_\infty = \psi\sigma_0\left[1 - \frac{2}{\exp(\varphi t) + \exp(-\varphi t)}\right] = \psi\sigma_0\left[1 - \frac{1}{\cosh(\varphi t)}\right] \qquad (3)$$

and the latter from Equation 2, taking $y = t$:

$$\tau_\infty = a\varphi\psi\sigma_0\left[\frac{\exp(\varphi t) - \exp(-\varphi t)}{\exp(\varphi t) + \exp(-\varphi t)}\right] = a\varphi\psi\sigma_0\tanh(\varphi t) \qquad (4)$$

2.2. Failure mechanisms at the platelet/matrix interface

The following analysis considers that the platelets possess a perfect-planar orientation in the composite material. The approach used to model the strength of such a composite with transverse isotropy is based on the critical element model developed by Reifsnider [37, 38]. The failure of the critical element controls the failure of the composite part, and is chosen identical to the single-platelet matrix element used for the stress transfer model, shown in Fig. 1. In this geometry, it is clear that a crack initiated perpendicular to the surface when the composite is loaded in flexion will reach a platelet.

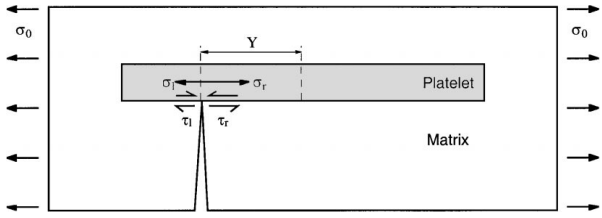

Figure 2 Schematics of the stress field in the vicinity of a matrix crack tip perpendicular to the platelet/matrix interface, when the matrix element is loaded in tension.

At this point, and depending on the stress state and on the strength of the platelet and of the interface, the crack moves further, crossing the particle, or deviates, and causes delamination at the interface. The stress state acting on the platelet at the crack tip, as sketched in Fig. 2, not only depends on the platelet length, but also on the distance Y between the crack tip and the center of the particle, i.e., on the lengths of the platelet parts lying to the left and right of the crack tip.

On the one hand, the platelet axial stress at the location Y of the crack, σ_{crack}, is determined by the axial stress state in both parts of the platelet. Due to the asymmetry of the loading geometry with respect to the y-axis, an accurate determination of σ_{crack} would require numerical methods, which is outside the scope of the present work. Alternatively, one may consider upper and lower bounds to the stress state. In the former case, σ_{crack} is equal to the sum of the maximum axial stresses acting on each part of the particle:

$$\sigma_{\text{crack}} = \psi\sigma_0\left[2 - \frac{1}{\cosh(\varphi\cdot(t-Y)/2)} - \frac{1}{\cosh(\varphi\cdot(t+Y)/2)}\right] \quad (5)$$

In the latter case, σ_{crack} would be equal to the sum of the average stresses acting on each part of the particle, with the further assumption of a symmetric loading geometry, i.e., two cracks are present on both sides of the platelet at the same location Y. It was found in fact that these two bounds lead to differences of less than 5% in σ_{crack} values, for platelets longer than approx. 15 μm. Since the effect of such small differences on the calculated composite strength is less than the typical experimental scatter, the following will only consider the upper bound approach, as expressed by Equation 5.

On the other hand, the largest shear stresses acting at the interface in the presence of a crack, lie on the side where the crack is farthest from the platelet edge:

$$\tau_{\text{crack}} = a\varphi\psi\sigma_0\tanh(\varphi\cdot(t+Y)/2) \quad (6)$$

The profiles of Equations 5 and 6 as a function of crack type distance from platelet center are shown for different particle lengths in Fig. 3. The profiles were calculated in the case of a poly(ethylene terephthalate) (PET) matrix, of elastic modulus $E_m = 3.7$ GPa and Poisson's ratio $\nu_m = 0.3$ and a silicon oxide (SiO_x) platelet of elastic modulus $E_p = 79.9$ GPa, and thickness $2a = 100$ nm, the ratio b/a being fixed to 10 [5]. This material system will be used to test the model prediction, and is detailed in the experimental section. As shown in Fig. 3, it is evident that, in the case of SiO_x platelets smaller than 8 μm, the tensile stress in the particles strongly depends on the position of the crack tip. By contrast, for larger platelets, the crack tip position only affects the tensile stress when the crack appears close to the edge of the particle. This trend is even clearer when looking at the shear stress acting at the interface in the vicinity of the crack tip, which shows no dependence on the crack tip position for platelets larger than 5 μm.

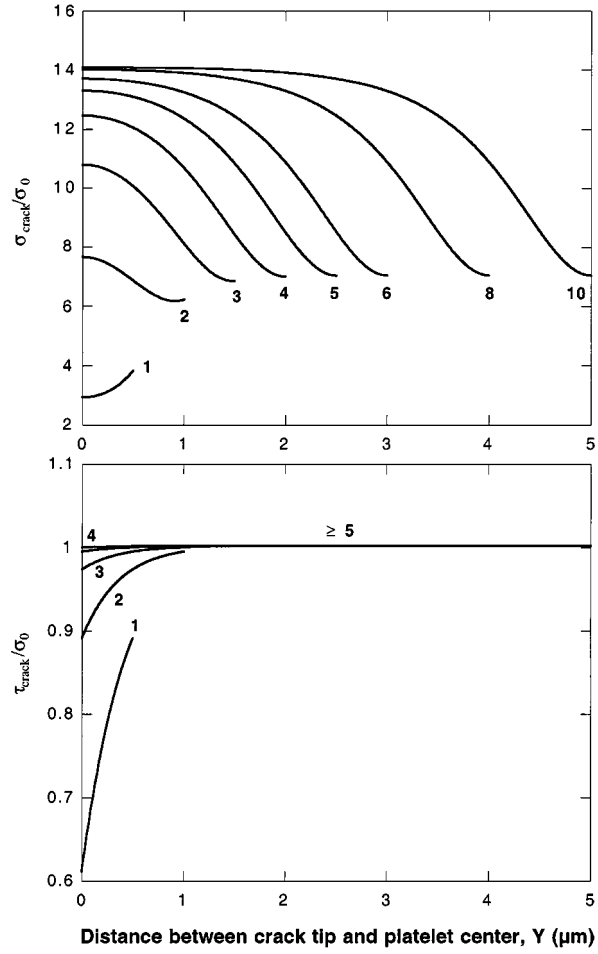

Figure 3 Normalized platelet tensile stress (top), and platelet/matrix interface shear stress (bottom), at the crack tip as a function of its position with respect to the center of the platelet. The values were calculated for a polyethylene terephthalate (PET) matrix and a silicon oxide (SiO_x) platelet, with properties as indicated in the text. The numbers in the figures correspond to the platelet length in μm.

2.3. The critical toughening transition in platelet-reinforced composites

For a given platelet length and crack tip position, it is possible to determine the failure mechanism that will govern the rupture of the composite by comparing both the tensile stress in the platelet derived from Equation 5 to its strength, $\sigma_{\max}$, and the shear stress calculated from Equation 6 to the interfacial shear strength, τ. When a crack reaches a platelet, four different cases can be identified, depending on the stress and strength states at the crack tip:

i) $\tau_{crack} < \tau$ and $\sigma_{crack} < \sigma_{max}$. In this case, the crack does not propagate since the stresses acting on platelet and interface are smaller than their respective strengths.

ii) $\tau_{crack} = \tau$ and $\sigma_{crack} = \sigma_{max}$. In this case, both interface shear strength and platelet tensile strength are reached at the same time. This situation which does not allow for the determination of the failure mechanism, is obviously very unlikely and has been disregarded in this work.

iii) $\tau_{crack} < \tau$ and $\sigma_{crack} = \sigma_{max}$. In this case, the platelet strength is reached before the interface shear strength, and the crack propagates by rupture of the platelet. This condition is written as $\sigma_{crack}/\tau_{crack} > \sigma_{max}/\tau$, which, using Equations 5 and 6, gives:

$$\frac{\left[2 - \dfrac{1}{\cosh(\varphi \cdot (t - Y)/2)} - \dfrac{1}{\cosh(\varphi \cdot (t + Y)/2)}\right]}{a\varphi \tanh(\varphi \cdot (t + Y)/2)} > \frac{\sigma_{max}}{\tau} \quad (7)$$

iv) $\tau_{crack} = \tau$ and $\sigma_{crack} < \sigma_{max}$. In this last case, in contrast to the previous case, the interface shear strength is reached before the platelet strength, and the crack propagates through interfacial delamination. This condition is written as $\sigma_{crack}/\tau_{crack} < \sigma_{max}/\tau$, which, using Equations 5 and 6, gives:

$$\frac{\left[2 - \dfrac{1}{\cosh(\varphi \cdot (t - Y)/2)} - \dfrac{1}{\cosh(\varphi \cdot (t + Y)/2)}\right]}{a\varphi \tanh(\varphi \cdot (t + Y)/2)} < \frac{\sigma_{max}}{\tau} \quad (8)$$

The left hand side of Equations 7 and 8 is plotted in Fig. 4 as a function of the distance of the crack tip from the particle center, normalized to the platelet length, for platelet aspect ratios ranging from 5 to 1000. The same parameter values as those shown in Fig. 3 were used. It is obvious that the ratio between the tensile stress in the platelet and the interface shear stress decreases drastically with decreasing platelet aspect ratio. Consequently, there exists a certain platelet length below which the condition for platelet rupture is never fulfilled, and in this case rupture always occurs through interface delamination. Further, except for very small particles, a strong dependence on the position of the crack tip is observed.

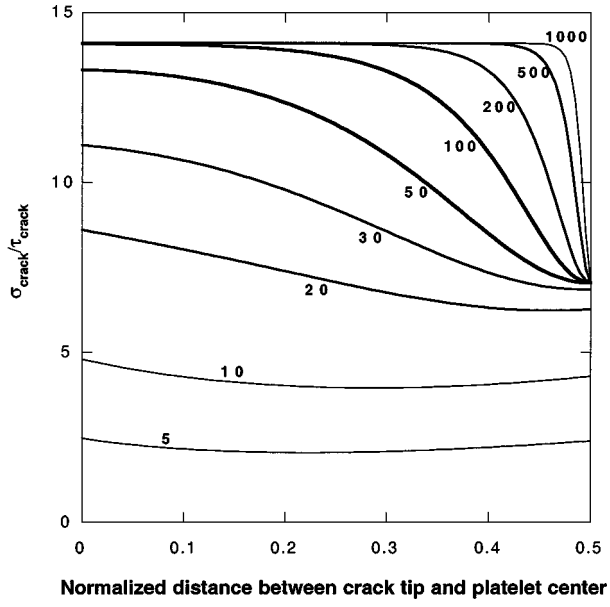

Figure 4 Ratio between tensile stress and shear stress at the crack tip shown in Fig. 3, as a function of the crack tip position with respect to particle center, normalized to the platelet length. The numbers in the figure correspond to the platelet aspect ratio.

The right hand side of Equations 7 and 8 represents an intrinsic property of the platelet/matrix system. The strength σ_{max} of brittle reinforcements has often been modeled as a function of their size, following Weibull statistics [39], whereas the interface shear strength τ is usually derived from adhesion tests (e.g., reference [40]). Assuming a constant value for τ and a Weibull dependence of the platelet strength, as was determined in a separate work [41], the ratio σ_{max}/τ decreases with platelet length, whatever the Weibull parameters and the value of the interface shear strength.

For larger platelets, the position of the crack tip with respect to the center of the particle will influence the failure mechanism, changing from platelet rupture to interface delamination when moving towards the edge of the particle. Considering that the crack appears at a random location, the probability Ω of the failure mechanism occurring through particle rupture is calculated from $\Omega = t/Y_c$, where Y_c is the crack position that satisfies the following implicit equation:

$$\frac{\left[2 - \dfrac{1}{\cosh(\varphi \cdot (t - Y_c)/2)} - \dfrac{1}{\cosh(\varphi \cdot (t + Y_c)/2)}\right]}{a\varphi \tanh(\varphi \cdot (t + Y_c)/2)} = \frac{\sigma_{max}}{\tau} \quad (9)$$

This probability is plotted as a function of platelet length in Fig. 5, using the case of SiO_x platelets in PET, for which experimental values of strength and adhesion had been determined in a separate study [41, 42]. It is clear that, up to a length of approx. 21 μm, the probability of failure through platelet rupture is zero, i.e., delamination of the interface will occur whatever the position of the crack. At higher lengths, this probability rises very rapidly, to reach 50% below 22 μm, and 90% below 40 μm. In the case of the PET/SiO_x system, the platelet length, ξ, at which the transition between platelet rupture and interface delamination occurs is thus very clearly in the vicinity of 21 μm. For comparison, the lower bound approach to the platelet stress σ_{crack} described in the previous section leads to a value of ξ equal to 22.5 μm. In case of other material combinations, the critical length at which this transition would occur should be determined from Equation 9. This marked transition, ξ, will be referred to as the critical toughening transition.

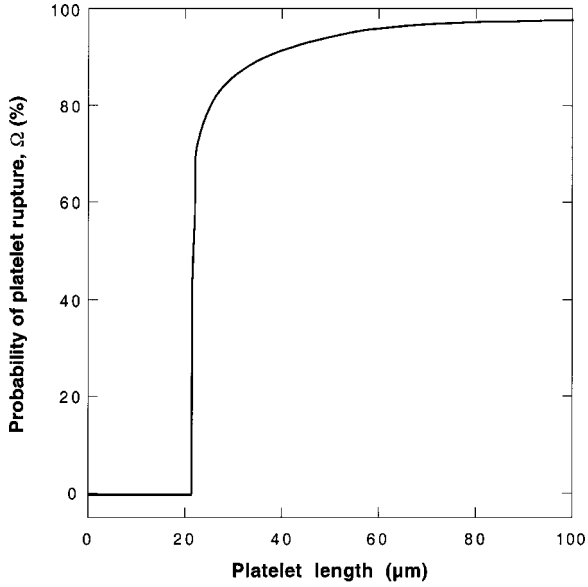

Figure 5 Probability of platelet rupture as a function of platelet length in the case of a polyethylene terephthalate (PET) matrix and a silicon oxide (SiO_x) platelet, with properties as indicated in the text.

2.4. Effect of process-induced internal stresses on failure mechanisms

The internal stresses which develop in the different phases when processing the composite material act in compression on the platelets, and in tension in the matrix, in the vicinity of the interface. In the presence of a crack, the stress relaxation in the matrix locally induces tensile stresses in the particle, which add to the applied stress. The increase of interfacial shear strength, resulting from higher compressive internal stress [43], will obviously affect the value of the transition ξ. To investigate the relation between internal stress and ξ, the RHS of Equation (9) is rewritten $\sigma_{max}/(\tau + \tau_i)$, where the internal shear stress τ_i was found to be proportional to the platelet compressive stress σ_i [43]. For the PET/SiO_x system introduced earlier, the result of the computation is shown in Fig. 6, as a function of the normalized interface shear strength. It is obvious that the critical toughening length is highly dependent on internal stress. Such process-induced stresses are therefore likely to change the failure mechanism acting on the composite.

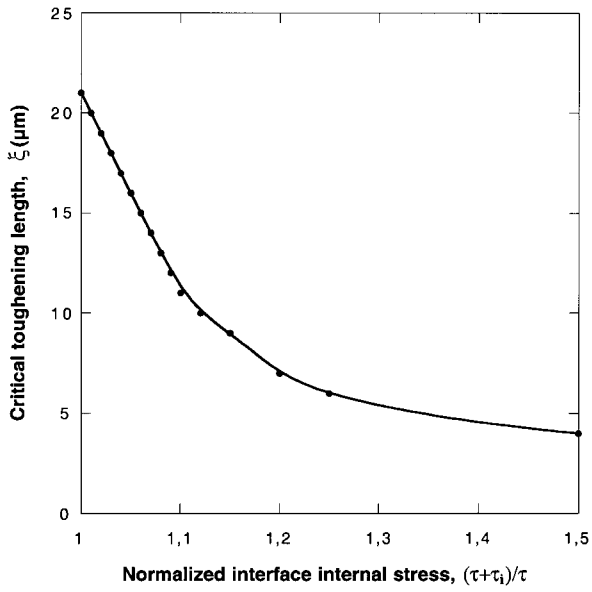

Figure 6 Evolution of the critical toughening length as a function of the interface internal stress normalized to the value of the interface shear strength. Dots were computed from Equation (9), at five levels of internal stresses, and the line is a guide for the eye.

2.5. Tensile strength of platelet-reinforced composites. The case of platelets smaller than the critical toughening length

The composite strength when the platelets are smaller than the critical toughening length is derived from Equations 6 and 9. In this case, which always corresponds to the interface delamination mechanism as was shown in Fig. 5, the interface stress depends to a large extent on the position of the crack along the platelet length. Assuming a random situation, the strength of the composite is calculated as the average over platelet length of the shear stress generated at the crack tip:

$$\sigma_c(L < \xi) = 2\frac{\tau + \tau_i}{aL\varphi\psi}\int_0^t [\tanh\{\varphi \cdot (t + y)/2\}]^{-1}\,dy$$
$$= 4\frac{\tau + \tau_i}{aL\varphi^2\psi}[\log\sinh(\varphi L/2) - \log\sinh(\varphi L/4)] \quad (10)$$

2.6. Tensile strength of platelet-reinforced composites. The case of platelets larger than the critical toughening length

Similarly to the above case, the strength of the composite with platelets larger than the critical toughening length is derived from Equations 5 and 9. However, this situation is more complicated since the probability of platelet delamination is not nil, as indicated in Fig. 5. Assuming a random situation, the composite strength is then written as:

$$\sigma_c(L > \xi) = (1 - \Omega)\cdot\sigma_c(L < \xi) + \Omega\cdot\sigma_c(L > \xi) \quad (11)$$

where the probability of platelet rupture, Ω, and the critical length, ξ, depend on the internal stress. The first term of the RHS in Equation 11 represents the contribution of platelets when the crack comes close to an edge, which corresponds to the case of small platelets treated by Equation 10. The second term of the RHS represents the contribution of platelets which fail without delamination, and the strength $\sigma_c(L > \xi)$ is integrated over platelet length:

$$\sigma_c(L > \xi) = 2\frac{\sigma_{max}(L) - \sigma_i}{\Psi L}\int_0^t \times \frac{dy}{\left[2 - \frac{1}{\cosh(\varphi\cdot(t - y)/2)} - \frac{1}{\cosh(\varphi\cdot(t + y)/2)}\right]} \quad (12)$$

where $\sigma_{max}(L)$ represents the dependence of platelet strength on its length, which, in the present case, was

modeled assuming a two-parameter Weibull distribution. Further details on the strength distribution of the oxide platelets can be found in ref. [41]. When the platelets are significantly larger than the critical toughening length, typically for aspect ratios larger than several thousands, the probability that a crack will appear at the platelet edge becomes negligible, and the composite strength simplifies to:

$$\sigma_c(L > \xi) = \frac{\sigma_{max}(L) - \sigma_i}{2\Psi}\left[1 - \frac{1}{\cosh(\varphi L/4)}\right]^{-1} \quad (13)$$

To verify the accuracy of the model, platelet-reinforced composites were manufactured with well-controlled platelet lengths, as described in the following.

3. Short-term strength of platelet-reinforced composites. The case of compression molded materials

3.1. Materials, processing and testing methods

Two types of platelet-reinforced composites were manufactured by compression molding stacks of 100 individual SiO_x coated PET films, in order to obtain composite materials with a perfect planar orientation of the ceramic platelets [44]. The thickness of the oxide coating was 100 nm, and that of the PET substrate 12 μm. The ratio of coating to substrate thicknesses corresponds to the volume fraction of the platelets in the composite, equal to 0.83 vol%. In the first composite type, the length of all the platelets is larger than the critical toughening length ξ. In the second type, on the contrary, the length of all the platelets is smaller than ξ. It should be pointed out that the perfect parallel orientation of the oxide platelets mimics that of other platelets such as mica found in e.g., high-voltage electrical insulators. As was mentioned earlier, such well-defined planar geometry is also relevant for microelectronic assemblies, and it is therefore expected that the conclusions drawn from the study will be of widespread interest.

Stacking of the films was performed on a filament-winder on which a flat mandrel was mounted. The stacks were subsequently cut to fit into the mold (70×20 mm^2), with the length parallel to the machine direction of the film. The cut film stacks were dried overnight in a vacuum oven at 80°C prior to further processing. To avoid curling of the films, the stacks were submitted to slight pressure by covering them with glass sheets on which a light weight (approx. 10 g) was placed.

In order to obtain platelets with a length smaller than ξ, fragmentation of the oxide coating prior to processing was performed by stretching the film stacks to $25 \pm 0.5\%$ nominal strain. This procedure for accurately controlling of platelet length has been extensively detailed in recent works [41, 42], and yields platelets of lengths ranging from approx. 1 μm to 4 μm, with an average value of 2.5 μm, which is much smaller than the smaller value for ξ as shown in Fig. 6.

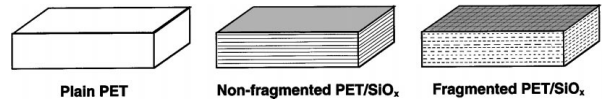

Figure 7 Layered PET/SiO_x composites compression molded from stacks of 100 films.

Platelets with lengths larger than ξ were obtained during the heating stage of the compression molding process described in the following. During this treatment, the continuous oxide layers failed due to the mismatch in the coefficients of thermal expansion between the polymer and the oxide, resulting in large platelets of length of the order of several 100 μm, which is significantly greater than ξ whatever the level of internal stress.

As depicted in Fig. 7, the composites in which the particle size is controlled will be referred to as "fragmented compression molded" and the composites prepared without this treatment as "non-fragmented compression molded". For comparative purposes, a reference, plain PET compression molded material was manufactured from stacks of 100 non-coated PET films, following strictly the same conditions as for the coated films. The corresponding material will be referred to as "plain compression molded" material.

The film stacks were compression molded on a servo-hydraulic machine (Interlaken Inc.). A matched die mold with built in heating and cooling systems was mounted on this frame. The mold dimensions were 70×20 mm^2. The upper and lower surfaces of the mold were covered with Kapton® tape to prevent the polymer sticking to the metal. The film stacks were placed in the cold mold, and submitted to a pressure of 1.8 MPa. The molds were then heated to a temperature of 260 °C, at which point the pressure was raised to 8 MPa, and held at this value for 60 seconds. The system was then cooled under pressure to room temperature and the parts demolded. The thickness of the resulting compression molded specimens was approximately 1.1 ± 0.05 mm for the plain and non-fragmented specimens, and 0.95 ± 0.06 mm for the fragmented ones.

Using a slow diamond circular saw (approx. 60 rpm), the samples were finally cut in two parts along their length, in order to obtain a width of 10 mm suitable for mechanical testing. After processing, the specimens were stored in a freezer at −18 °C until testing, to avoid structural changes in the materials. The structural state of the PET in the plain material and the two types of composites was analyzed by means of differential scanning calorimetry (DSC) at heating and cooling rates of 10 K/min. The results reported in Table I show that

TABLE I Structural state of the PET in the compression molded materials

Compression molded material	Glass transition temperature (°C)	Melting peak (°C)	Initial crystallinity (%)	Crystallisation temperature* (°C)
Plain	75.5	258.6	33.5	206.6
Non-fragmented	76.7	261.2	36.4	206.1
Fragmented	73.9	256.4	32.4	207.0

(*) upon cooling from the melt at 10 K/min.

the plain, fragmented, and non-fragmented compression molded materials possess similar glass transition temperature and crystallinity. In other words, any difference in mechanical behavior between the two types of composites with the same volume fraction of oxide platelets should be attributed to differences in platelet size and stress state.

The compression molded composite specimens were tested at room temperature by means of a 3-point-bending test on a screw-driven tensile testing machine (UTS). The rods used were 5 mm in diameter and the span width was set to 25 mm. The crosshead speed was 0.5 mm/min, corresponding to a strain rate on the outer layers of approx. $8 \cdot 10^{-5}$ s^{-1}.

3.2. Validity of the stress transfer model

A first step in the analysis of the theoretical derivation presented in the previous section is to verify the validity of the stress transfer equations. To this end, the stress in every platelet is calculated as a function of its length using Equation 1, and, knowing the platelet length distribution, the contribution of the platelets to the total stress is calculated. The platelet length distribution was carefully measured during the fragmentation process, as detailed elsewhere [41, 42]. Adding this stress to the tensile stress measured during the 3-point-bending test of the plain material, σ_{plain}, the tensile stress of fragmented compression molded material, σ_{frag}, is molded following:

$$\sigma_{\text{frag}}(\varepsilon) = (1-\Phi)\sigma_{\text{plain}}(\varepsilon) + \Phi \sum_{L} (\Phi_L \sigma(\varepsilon, L)) \quad (14)$$

where ε is the applied strain, Φ is the volume fraction of platelets and Φ_L is the volume fraction of platelets of length L.

Fig. 8 compares the experimental stress of a fragmented compression molded sample, to the stress calculated at different strains according to Equation 15, with the same elastic constants of the PET and the oxide, as reported in Section 2. The excellent agreement between experimental and calculated values shows the relevance of the elastic approach to stress transfer adopted in the study.

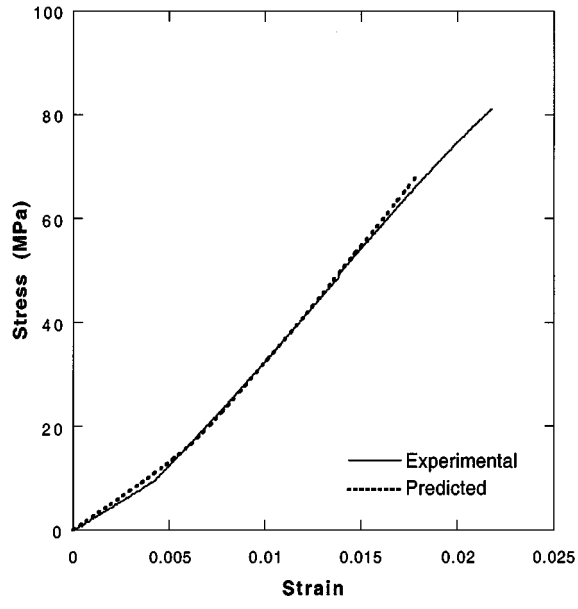

Figure 8 Experimental (line) and modeled (dots) flexural stress versus strain curves of the fragmented compression molded composite.

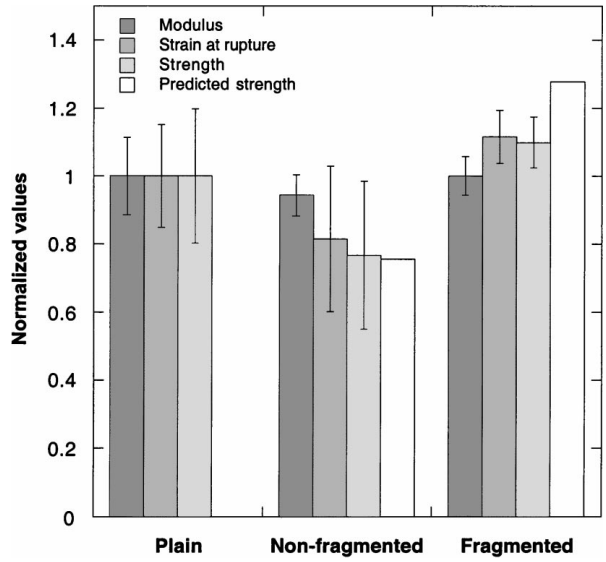

Figure 9 Mechanical properties of the compression molded PET/SiO_x composites normalized to the plain reference PET properties.

3.3. The critical toughening transition

The elastic moduli, strain at rupture, and strength of the plain PET, non-fragmented and fragmented compression molded platelet-reinforced PET are reported in Table II. None of the samples presents ductile behavior. This is primarily due to the high crystallinity of the polymer, and to the large size of the crystals induced by the low cooling rate, which has been shown to embrittle PET significantly [45]. Nevertheless, the benefit of reducing the platelet size is striking, as shown in Fig. 9, which presents the mechanical properties of the three materials normalized to the values obtained for plain PET. In fact, the fragmented compression molded material is stronger than plain PET, whereas the non-fragmented compression molded material fails at lower stress and strain values. The toughness of the composite materials was calculated as a first approximation as half the product of strain at rupture times strength. The increase in toughness of the fragmented material, compared with the non-fragmented material, achieved through platelet size control, is found to be as high as approx. 100%. Furthermore, the scatter in the experimental data obtained for the fragmented compression

TABLE II Mechanical properties of the compression molded materials

Compression molded material	Modulus (GPa)	Strength (MPa)	Strain at rupture (%)
Plain	3.5 ± 0.4	60.0 ± 11.9	1.73 ± 0.26
Non-fragmented	2.9 ± 0.3	46.0 ± 10.0	1.40 ± 0.30
Fragmented	3.5 ± 0.2	65.9 ± 4.5	1.93 ± 0.14

molded material is the lowest of all three materials, indicating a higher reliability of the composite reinforced with platelets smaller than the critical toughening length.

Fig. 9 also compares the experimental and predicted strengths (Equations 10 and 13), calculated with the same PET/SiO_x parameters as indicated previously. In the case of the non-fragmented compression molded composite, the internal stress was calculated as a thermoelastic stress, neglecting stress relaxation effects:

$$\sigma_i = \Delta\alpha \cdot (T_s - T_g) \cdot E_p \qquad (15)$$

where $\Delta\alpha$ is the difference between the coefficients of thermal expansion of the platelet and the polymer matrix, T_g is the glass transition temperature of the polymer, T_s is the service temperature, and E_p is the elastic modulus of the platelet. The result is a compressive stress equal to -160 MPa, with the coefficient of thermal expansion of the PET equal to $3.6 \cdot 10^{-5}\ ^\circ C^{-1}$ and neglecting that of the oxide [43].

Taking the strength σ_{max} of very large platelets equal to 800 MPa [43], the strength of the non-fragmented material is predicted to equal 45.3 MPa, whereas the average experimental strength is found to be equal to 46.0 MPa. This remarkable agreement, with a difference of less than 2%, shows the importance of process-induced internal stresses on the failure mechanisms in platelet-reinforced composites.

In the case of the fragmented compression molded composite, the PET/SiO_x interfacial shear strength which intervenes in Equation 10 was taken to be equal to 76.9 MPa, as had been measured on an individual PET/SiO_x film [43]. The internal shear stress was further assumed to be negligible, since all the platelets are smaller than the critical stress transfer length [41]. The strength of the fragmented compression molded material is predicted to equal 76.7 MPa, whereas the experimental strength is found to be equal to 65.9 MPa. The model overestimates the experimental value by 14%, which is slightly beyond the typical error of 12% found in the measurement of PET/SiO_x interfacial adhesion [41]. Nevertheless, the toughening effect of the small platelets obtained experimentally, which is predicted by the model, demonstrates the importance of an accurate determination of the platelet/polymer adhesion in modeling the strength of the composite.

4. Short-term strength of platelet-reinforced composites. The case of injection molded materials

4.1. Materials, processing and testing methods

Injection molded composites were processed from the same PET/SiO_x films as described in the preceding section. The oxide platelets generated during the processing operation described thereafter present a size distribution, and a range of orientations in the molded specimens which is typical of foreign particles diluted in recycled polymers. These contaminants act as stress concentrators that often embrittle the recycled material [46, 47]. Knowledge about the influence of the morphology and stress state of the platelets on the strength of the injection molded composites is expected to provide tools to tailor the reprocessing of polymers, as, for instance, the design of melt filtration during extrusion.

The films were fed into an extruder to obtain pellets, which were subsequently injection molded into test specimens. An in-line drying tower in which dry air was blown at 120 °C was built and directly connected to the extruder to prevent hydrolysis of the PET [43]. By means of Karl-Fischer titration (Mettler DL18), the water content of the polymer when entering the extrusion hopper was measured to be equal to 70 ± 50 ppm, which is close to the limit value given in the literature [48]. Extrusion was carried out at 50 rpm on a table-top co-rotating twin screw extruder with a screw diameter of 16 mm, and length to diameter ratio equal to 16 (PRISM TSE16-TC). The respective feed, melting and nozzle temperatures were set to 210 °C, 245 °C and 235 °C.

The extrudate was pelletized into 2 mm diameter and 4 mm long pellets, which were dried overnight in a vacuum oven at 80 °C prior to injection molding on a Buttler 10/90V miniinjection molder. The feed zone was set at 260 °C and melting zone at 285 °C. Injection was performed at 90 MPa, in a mold temperature controlled to 30 °C, in which the pressure was kept for 18.5 s at 35 MPa. The tensile test injection molded specimens were 55 mm long and 3 mm thick. The gauge dimensions were 10 mm in length and 3 mm in width.

Similarly to the compression molded materials, the size of the oxide platelets in the injection molded specimens was controlled by stretching the film to 25% strain prior to feeding into the drying tower of the extruder. In this case all the platelets were smaller than ca. 4 μm. The corresponding materials will be referred to as "fragmented injection-molded". Without this treatment, the length of the platelets is in the range of 10–100 μm, due to attrition during the extrusion step, and the resulting materials will be referred to as "non-fragmented injection-molded". Reference specimens were also processed out of plain PET.

The structural state of the PET in the injection molded materials was analyzed by means of DSC under the same conditions as those indicated in the preceding section. The samples were systematically cut from a whole section of the specimens in the gauge section. An exothermic cold-crystallization event was observed on all three material types at a temperature of approx. 128 °C. This feature was due to the low degree of crystallinity induced by the cooling rate higher than 20 K/s involved in the injection molding process [49, 50]. The initial crystallinity of the injection molded materials was calculated by deducing the area of the cold-crystallization peak from the area of the melting peak. The salient values for the three types of injection molded materials are reported in Table III. These values are close enough to each other so that any difference in mechanical properties would result from the different morphologies of the platelets.

The injection molded specimens were tested at room temperature under uniaxial tension at a strain rate of $1.25 \cdot 10^{-2}\ s^{-1}$ on a screw-driven tensile testing machine (Zwick) under displacement control,

TABLE III Structural state of the PET in the injection molded materials

Injection molded material	Glass transition (°C)	Cold crystallization (°C)	Melting peak (°C)	Initial crystallinity (%)	Crystallisation temperature* (°C)
Plain	72.6	128.9	258.9	18.2	203.4
Non-fragmented	72.2	127.4	259.8	16.7	205.0
Fragmented	72.5	127.6	258.2	16.9	204.3

(*) upon cooling from the melt at 10 K/min.

and equipped with a 1 kN load cell. An extensometer was used to measure the deformation of the material in the gauge region. Due to the high deformations involved and the development of a neck, true stress and strain were computed from the nominal values following: $\varepsilon_{\text{true}} = \ln(1 + \varepsilon)$ and $\sigma_{\text{true}} = \sigma \exp(\varepsilon_{\text{true}})$.

4.2. The brittle-to-ductile transition in platelet-reinforced composites

During its residence time in the extruder, the partially molten PET/SiO_x material undergoes intense shear rates that break the oxide layer into flake-like platelets, which are dispersed into the PET through the mixing effect of the co-rotating screws. The material then solidifies prior to being cut into pellets. This pelletizing does not further reduce the size of the platelets, as they are already considerably smaller than the pellet size. During subsequent injection molding, the PET/SiO_x composite is remelted and injected into a cold mold. Again, high shear rates are involved and the size of the platelets is likely to be further reduced, whereas their orientation in the flow direction is increased.

By contrast, in the case of fragmented films, the SiO_x platelets are initially extremely small prior to processing and their size will not be significantly modified during the different processing stages.

The orientation distribution of platelets within both fragmented and non-fragmented injection molded specimens is far from the perfect-planar orientation of the compression molded composites. Nevertheless, the very different size of platelets between the two types of injection molded specimens is expected to influence their mechanical properties. Fig. 10 compares the tensile behavior of the two types of materials with that of plain PET. Up to yield, the different material types behave similarly, with elastic moduli and yield stresses being equal within experimental scatter. The initial SiO_x layer forms individual platelets, with aspect ratios of the order of several 100 in the case of the non-fragmented material, and close to 25 in the case of the fragmented material. Acting in a similar way to short fibers in reinforced composites, but in addition being diluted to less than 1 vol% in the polymer, this platelet structure have limited effect on the stiffness of the material. Nevertheless, a spectacular difference is evident in the strain at rupture and strength of the different injection molded material types. Plain PET and fragmented materials present a very ductile behavior while the non-fragmented material exhibits a brittle rupture at less than 4% strain. Also noticeable was the fact that the compression molded and injection molded materials possess considerably different ductilities, with

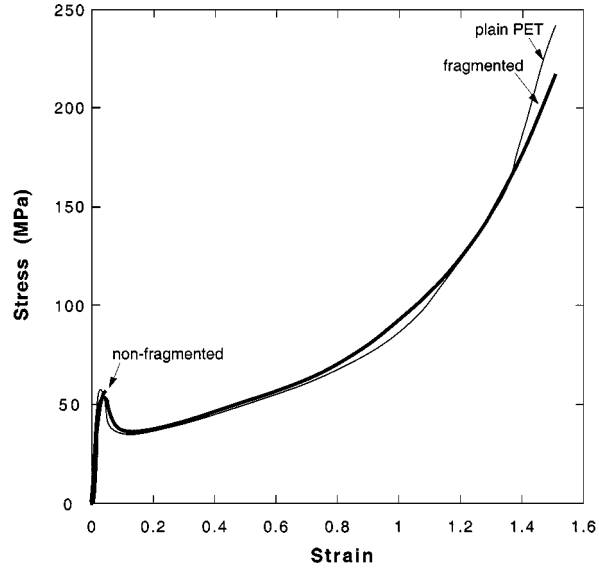

Figure 10 Tensile behavior of the injection molded PET and PET/SiO_x composites.

the exception of the non-fragmented composites which are all brittle. This difference is due to the different crystalline structures of the PET matrix induced upon cooling in the two processing techniques.

The theoretical treatment developed in this study is only valid in the elastic range, and is therefore limited to the non-fragmented injection molded material, which fails without extensive yield. Furthermore, to be applicable, the model geometry should account for the platelet orientation distribution resulting from injection molding. The experimental results nevertheless indicate the considerable importance of particle size regarding the mechanical properties of polymers, specifically at dilute fractions of platelets, such as contaminants present in recycled materials.

Ongoing work is devoted to refining the stress transfer modeling, and accounting for the radial-dependence of the matrix axial stress [51]. This approach avoids the introduction of the adjustable size of the matrix element, b, which was set arbitrarily to a value of $10 \cdot a$ in the model. Further research is currently investigating the influence of time-dependent effects such as viscoelastic relaxation and structural recovery [52] on the internal stress state, which were reported to profoundly affect the overall long-term failure response of PET/SiO_x composites [44] and epoxy/glass composites [53].

5. Conclusions

The short-term mechanical strength of platelet-reinforced polymer composites, which are of interest

for structural components, electrical insulators or recycled plastics, was modeled using classic two-dimensional elastic stress transfer analysis. The approach assumes that the failure of the composite is controlled by the failure of a critical element containing a single platelet embedded in a matrix element, with a matrix crack perpendicular to the platelet/matrix interface. Two key failure mechanisms were defined as platelet rupture or interface delamination. The stress state in the platelet, and at the platelet/matrix interface in the vicinity of the crack tip, were calculated accounting for the tensile strength and adhesion of the platelet to the matrix, as well as process-induced internal stresses.

The model predicts the existence of a platelet length below which interface delamination will always occur, thus toughening the composite, and above which the dominant failure mechanism will on the contrary be the rupture of the platelet. The platelet length at which the critical toughening transition occurs depends on the ratio of platelet strength and platelet/matrix interfacial strength, on the elastic properties of the platelet and matrix, and on the internal stress state, all of which can be determined by means of separate experiments.

The approach was applied to 0.83% vol silicon oxide platelets/poly(ethylene terephthalate) composites, where the size of the platelets was accurately controlled either below or above the predicted critical length. Compression molded composites with perfect alignment of the platelets, representative of electrical insulation and microengineering applications, and injection molded composites, representative of recycled polymers, were manufactured and tested. The strength of the compression molded composites was found to be accurately predicted by the strength model, and a 100% increase in toughness in the case of platelets smaller than the critical length was measured, compared to that of larger platelets. Injection molded composites with platelets larger than the critical length were found to fail without yielding. By contrast, when the platelets were smaller than the critical length, the injection molded composites exhibited excellent ductility. The general agreement obtained between the predicted and observed toughening transition shows the importance of filler size and internal stress state on the strength of platelet-reinforced composites.

Acknowledgments

The authors gratefully acknowledge the Swiss Priority Program for Materials Research (PPM) for funding this work.

References

1. Y. S. CHOU and D. J. GREEN, *J. Amer. Ceram. Soc*. **76** (1993) 1452.
2. D. BARIL and M. K. JAIN, *Ceram. Eng. Sci. Proc.* **12** (1991) 1175.
3. M. HÄNNINEN, R. A. HABER and D. E. NIESZ, *Ceram. Trans*. **19** (1991) 749.
4. M. R. PIGGOTT, "Load Bearing Fiber Composites" (Pergamon Press, Elmsford, NY, 1980).
5. C.-H. HSUEH, *Compos. Eng*. **4** (1994) 1033.
6. H. KAHN and A. H. HEUER, *Materials Today* **2** (1999) 3.
7. S. AHMED and F. R. JONES, *J. Mater. Sci*. **25** (1990) 4933.
8. J. AVESTON and A. KELLY, *ibid*. **8** (1973) 352.
9. J.-P. FAVRE and D. JACQUES, *ibid*. **25** (1990) 1373.
10. L. A. GOETTLER *Polym. Compos.* **5** (1984) 60.
11. C.-H. HSUEH, *Mater. Sci. Eng*. **A123** (1990) 1.
12. *Idem., ibid*. **A125** (1990) 67.
13. *Idem., ibid*. **A145** (1991) 135.
14. *Idem., ibid.* **A145** (1991) 143.
15. *Idem., ibid.* **A154** (1992) 125.
16. *Idem., ibid.* **A159** (1992) 65.
17. *Idem., ibid.* **A165** (1993) 189.
18. *Idem., ibid.* **A161** (1993) L1.
19. A. KELLY and W. R. TYSON, *J. Mech. Phys. Sol*. **13** (1965) 329.
20. M. MIWA, T. OSHAWA and K. TAHARA, *J. Appl. Polym. Sci*. **25** (1980) 795.
21. M. NARDIN and J. SCHULTZ, *Compos. Interf*. **1** (1993) 177.
22. S. BARTA, *J. Appl. Phys*. **75** (1994) 3258.
23. A. J. KINLOCH, D. L. MAXWELL and R. J. YOUNG, *J. Mater. Sci*. **20** (1985) 4169.
24. D. MAXWELL, R. J. YOUNG and A. J. KINLOCH, *J. Mater. Sci. Letters* **3** (1984) 9.
25. A. C. MOLONEY, H. H. KAUSCH and H. R. STIEGER, *J. Mater. Sci*. **18** (1983) 208.
26. B. PUKÁNSZKY, *Makromol. Chem. Macromol. Symp.* **70/71** (1993) 213.
27. E. SIDERIDIS and G. PAPANICOLAOU, *Rheol. Acta* **27** (1988) 608.
28. J. W. SMITH, W. J. CANTWELL, A. DEMARMELS and H. H. KAUSCH, *J. Mater. Sci*. **26** (1991) 5534.
29. J. SPANOUDAKIS and R. J. YOUNG, *ibid*. **19** (1984) 473.
30. *Idem., ibid.* **19** (1984) 487.
31. L. A. VRATSANOS and R. J. FARRIS, *Polym. Eng. Sci*. **33** (1993) 1466.
32. *Idem., ibid.* **33** (1993) 1458.
33. H. L. COX, *Br. J. Appl. Phys*. **3** (1952) 72.
34. C. H. HSUEH, *Acta Mater*. **46** (1998) 2131.
35. W. R. TYSON and G. J. DAVIS, *Brit. J. Appl. Phys*. **6** (1965) 2038.
36. S. P. TIMOSHENKO and J. N. GOODIER, "Theory of Elasticity" (McGraw Hill, New York, 1951).
37. K. L. REIFSNIDER and W. W. STINCHCOMB, in "Composite Materials: Fatigue and Fracture," edited by H.T. Hahn (ASTM, Philadelphia, PA, 1986).
38. K. REIFSNIDER, N. IYENGAR, S. CASE and Y. L. XU, in Durability Analysis of Structural Composite Systems, edited by A. H. Cardon, (A. A. Balkema, Rotterdam, NL, 1996).
39. W. WEIBULL, *J. Appl. Mech*. **18** (1951) 293.
40. M. J. PITKETHLY, J. P. FAVRE, U. GAUR, J. JAKUBOWSKI, S. F. MUDRICH, D. L. CALDWELL, L. T. DRZAL, M. NARDIN, H. D. WAGNER, L. DILANDRO, A. HAMPE, J. P. ARMISTEAD, M. DESAEGER and I. VERPOEST, *Compos. Sci. Technol*. **48** (1993) 205.
41. Y. LETERRIER, L. BOOGH, J. ANDERSONS and J.-A.E. MÅNSON, *J. Polym. Sci. B: Polym. Phys*. **35** (1997) 1449.
42. Y. LETERRIER, J. ANDERSONS, Y. PITTON and J.-A. E. MÅNSON, *ibid*. **35** (1997) 1463.
43. Y. WYSER, Ph.D. thesis, EPFL #1750, 1997.
44. Y. LETERRIER, Y. WYSER and J.-A. E. MÅNSON, *J. Appl. Polym. Sci*. **73** (1999) 1427.
45. M. R. TANT and W. T. CULBERSON, *Polym. Eng. Sci*. **33** (1993) 1152.
46. D. VETTER, B. WAMPFLER and B. WÜST, in Proc. R'95 (Geneva, Feb. 1–3, 1995) p. 207.
47. P.-A. ERIKSSON, A.-C. ALBERTSSON, P. BOYDELL and J.-A. E. MÅNSON, *Polym. Eng. Sci*. **38** (1997) 749.
48. T. WHELAN and J. GOFF, "Injection Molding of Engineering Thermoplastics" (Van Nostrand Reinhold, New York, 1990).

49. K. T. NGUYEN and G. PREVOST, in Proc. ANTEC'93, 1995 p. 245.
50. L. QUINTANILLA, J. C. RODRIGUEZ-CABELLO, T. JAWHARI and J. M. PASTOR, *Polymer* **34** (1993) 3787.
51. D. A. MENDELS, Y. LETERRIER and J.-A.E. MÅNSON, *J. Compos. Mater*. **33** (1999) 1525.
52. J. M. HUTCHINSON, *Prog. Polym. Sci*. **20** (1995) 703.
53. D. A. MENDELS, Y. LETERRIER and J.-A. E. MÅNSON, in "Recent Developments in Durability Analysis of Composite Systems," edited by A. H. Cardon, H. Fukuda, K. L. Reisnider, G. Verchery (A. A. Balkema, Rotterdam, NL, 2000). p. 185.

Received 20 April
and accepted 18 September 2000